# Photochemical & Photobiological Sciences

Accepted Manuscript


This is an *Accepted Manuscript*, which has been through the Royal Society of Chemistry peer review process and has been accepted for publication.

*Accepted Manuscripts* are published online shortly after acceptance, before technical editing, formatting and proof reading. Using this free service, authors can make their results available to the community, in citable form, before we publish the edited article. We will replace this *Accepted Manuscript* with the edited and formatted *Advance Article* as soon as it is available.

You can find more information about *Accepted Manuscripts* in the Information for Authors.

Please note that technical editing may introduce minor changes to the text and/or graphics, which may alter content. The journal's standard Terms & Conditions and the Ethical guidelines still apply. In no event shall the Royal Society of Chemistry be held responsible for any errors or omissions in this *Accepted Manuscript* or any consequences arising from the use of any information it contains.

ROYAL SOCIETY OF CHEMISTRY

www.rsc.org/pps

Journal Name

RSCPublishing

ARTICLE

# Multi-component lanthanide hybrids based on zeolite A/L and zeolite A/L-polymer for tunable luminescence

Cite this: DOI: 10.1039/x0xx00000x

Lei Chen, Bing Yan*

Received 00th January 2012,
Accepted 00th January 2012

DOI: 10.1039/x0xx00000x

www.rsc.org/

Some multi-component hybrids based zeolite L/A are prepared. Firstly zeolite A/L are loaded with lanthanide complexes (Eu-DBM or Tb-AA (acetylacetone = AA, dibenzoylmethane = DBM)) into their channels. Secondly, 3-methacryloyloxypropyltrimethoxysilane (γ-MPS) is used to covalently graft onto the surface of functionalized zeolite A/L (Si-[ZA/L⊃Eu-DBM(Tb-AA)]). Thirdly, lanthanide ions ($Eu^{3+}$/$Tb^{3+}$) are coordinated to the functionalized zeolite A/L and ligands (phen (1,10-phenanthroline) or bipy (2,2'-bipyridyl)) are introduced by a ship-in-bottle method. The inner-outside double modifications of ZA/L with lanthanide complexes achieve the final hybrids and are characterized by means of XRD, FT-IR, UV-vis DRS, SEM and luminescence spectroscopy, some of which display white or near-white light emission. Furtherly, selected above hybrids are fabricated into PEMA/PMMA (poly ethyl methylacryate/poly methyl methacrylate) host to prepare luminescent polymer films. These results provide abundant data to be expected to have potential application in various practical fields.

## Introduction

In recent years, photofunctional lanthanide hybrid materials have aroused great interest of many researchers because of their outstanding optical properties and versatile potential applications such as optical amplifiers, NIR-emitting probes, fluorescent biology and light-conversion molecular devices.[1] These kinds of hybrid materials have the capability of coordinating synergy between the intrinsic characteristics of organic-inorganic hybrid hosts and the luminescent features of lanthanide ($Ln^{3+}$) ions.[2] $Ln^{3+}$ ions have the luminescence features of high luminescence quantum yield, ligand-dependent luminescence sensitization, long-lived emission, narrow bandwidth, large Stokes shifts. Moreover lanthanide organic-inorganic hybrid hosts have the intrinsic characteristics of thermal and chemical stability, optical and electronic properties, encapsulation of isolated emitting centers, biocompatibility and hydrophobic–hydrophilic balance.[1d,1e] Nevertheless, individual lanthanide ions normally display poor emission intensity due to their low absorption efficiency resulting from the forbidden nature of the f-f transition.

As a result, a number of investigations on lanthanide inorganic–organic hybrid materials incorporated lanthanide complexes in the inorganic matrices have been done during the last decade.[2] Among which some typical mesoporous and microporous systems such as MCM-41, SBA-15, periodic mesoporous organosilicas (POMs) and zeolites as the host have shown great potential and application.[3,4] Zeolites are a class of crystalline microporous materials, whose general formula can be represented as $M^{n+}_{x/n}[(AlO_2)_x\text{-}(SiO_2)_y]\cdot mH_2O$. The y/x ratio varies between 1 and 5, and their structure consists of are a rigid three-dimensional framework of tetrahedral $[AlO_4]^{5-}$ and $[SiO_4]^{5-}$ primary building units linked by oxygen bridges.[5] Zeolite L (ZL) contains of one-dimensional channels and strictly parallel channels arranged in a hexagonal framework. The channels have the smallest and the largest free diameters of 0.71 nm and 1.26 nm, respectively. Zeolite A (ZA) is structurally the most simple zeolite, it's channels have a smallest free diameter of about 0.41 nm, the largest diameter inside being 1.14 nm. Calzaferri and Li have done much research work in the field of fill the cavities and channels of zeolites with lanthanide compounds because of the fascinating luminescence properties of $Ln^{3+}$ ions.[6] Ln-ZA/L are obtained according to the ion-exchange synthesis procedure. The organic ligand has successfully been incorporated into the cavities and channels of zeolites, which has been known as "ship in a bottle method".[7] And another method is grafting lanthanide complexes on surface of zeolite crystals via Si-C covalent bonds.[8] The encapsulation of hybrid materials results in an excellent thermal stability of the complexes.[9] In this system, the typical emissions of $Ln^{3+}$ ions was greatly increasing via the so-called "antenna effect", defined as a light conversion process through an absorption by a ligand, energy transfer and emission by a lanthanide ion. However, as a host material, little attention has been paid to the luminescent properties of ZA hybrid materials, and hardly the comparison between ZA and ZL hybrid materials.[10] Besides, the multi-component assembly of different functional units with ZA/L can display the advantage of chemical modification and photofunctional tuning or integrating comparing the simple hybrids.

In this paper, we put forward a novel inside-outside double modification path to functionalize ZA/L host with lanthanide complexes and prepare the multi-component hybrid materials, which are named L-Ln-Si-[ZA/L⊃Eu-DBM] or L-Ln-Si-[ZA/L⊃Tb-AA]

Photochemical & Photobiological Sciences Accepted Manuscript

(acetylacetone = AA, dibenzoylmethane = DBM; Ln = Eu or Tb; L = phen (1,10-phenanthroline), bipy (2,2'-bipyridyl)). Besides, we also introduce PEMA/PMMA (poly ethyl methylacryate/poly methyl methacrylate) to prepare the polymer hybrid films. These hybrid systems not only show the versatile chemical modification to assemble multi-components, but also further realize the photofunctional integration with different units in the hybrids.

## Experimental section

**Materials.** Zeolite A (ZA) and Zeolite L (ZL) crystals were synthesized according to the reported procedure, and the potassium-exchanged form was used.[11] $TbCl_3{\cdot}6H_2O$ and $EuCl_3{\cdot}6H_2O$ were obtained by dissolving their respective oxides ($Tb_4O_7$ and $Eu_2O_3$) in hydrochloric acid (37 %). 3-methacryloyloxypropyltrimethoxysilane (97 %, γ-MPS, Lancaster), acetylacetone (98 %, AA, Aladdin), dibenzoylmethane (AR, DBM, Aladdin), sodium metaaluminate (Aladdin), sodium hydroxide (Aladdin), potassium hydroxide (Aladdin) and colloidal silica (40 %, Ludox HS-40, Sigma) were used as received. All the other reagents were analytically pure and purchased from China National Medicines Group.

**Physical characterization.** The X-ray powder diffraction patterns (XRD) were recorded on Rigaku D/max-Rb diffractometer equipped with Cu anode, the data were collected within the 2θ range of 5–60 °. Scanning electronic microscope (SEM) images were obtained with a Hitachi S-4800. The Fourier transform infrared spectra (FTIR) were measured within KBr disks from 4000 to 400 $cm^{-1}$ region using a Nexus 912AO446 infrared spectrum radiometer. Luminescent excitation and emission spectra of the samples were performed on Edinburgh FLS920 spectrophotometer. The outer luminescent quantum efficiency was determined using an integrating sphere (150 mm diameter, $BaSO_4$ coating) from Edinburgh FLS920 phosphorimeter. The spectra were corrected for variations in the output of the excitation source and for variations in the detector response. The absorption intensity was calculated by subtracting the integrated intensity of the light source with the sample in the integrating sphere from the integrated intensity of the light source with a blank sample in the integrating sphere. The ultraviolet–visible diffuse reflective absorption spectroscopy (UV–vis DRS) were acquired on B&WTEKO BWS003 UV-vis diffuse reflectance spectroscopy from 800 to 200 $cm^{-1}$.

**Synthesis of ZA/L⊃Eu-DBM and ZA/L⊃Tb-AA.** Ln-ZA/L (Ln = $Eu^{3+}$ or $Tb^{3+}$) was obtained according to the ion-exchange synthesis procedure as follows. A certain amount of zeolite A/L was added to 1.2 mL of a 0.05 M aqueous solution of $LnCl_3{\cdot}6H_2O$ and stirred for 12 h at 353 K. The product was collected by centrifugation, washed with deionized water by three times and then dried at 353 K under normal atmospheric conditions. The hybrid materials ZA/L⊃Eu-DBM and ZA/L⊃Tb-AA were prepared by ship-in-bottle method according to the reference.[9] Ln-ZA/L were firstly degassed and dried for 2 h at 423 K to get rid of the solvent molecules in zeolite channels, and then it was exposed to the DBM vapor at 453 K for 18 h, or exposed to AA vapor at 393K for 18h. The hybrid material was washed with $CH_2Cl_2$ by three times to remove only physically absorbed ligands, and then left in the oven at 333 K under vacuum.

**Modifications of ZA/L⊃Eu-DBM and ZA/L⊃Tb-AA with 3-methacryloyloxypropyltrimethoxysilane (γ-MPS).** 100 mg of ZA/L⊃Eu-DBM or ZA/L⊃Tb-AA was first dissolved in 20 mL toluene by stirring and then 0.6 mL γ-MPS was added to the solution dropwise. The whole mixture was refluxed in a covered flask under argon atmosphere at 383K for 20 h. The product was collected by centrifugation and washed with toluene, and then dried at 373 K overnight under vacuum.

**Preparations of L-Ln-Si-[ZA/L⊃Eu-DBM] and L-Ln-Si-[ZA/L⊃Tb-AA] (Ln = Eu or Tb; L = phen (1,10-phenanthroline), bipy (2,2'-bipyridyl)).** 90 mg modified zeolite (Si-[ZA/L⊃Eu-DBM] or Si-[ZA/L⊃Tb-AA]) was suspended in 25 mL of ethanol solution, then 0.5 mL of $LnCl_3{\cdot}xH_2O$ ethanol solution (0.1 $mol{\cdot}L^{-1}$) was added to the mixture dropwise, continuously stirring at 313bK for about 5 h. The product was obtained after centrifugation and drying obtained Ln-Si-[ZA/L⊃Eu-DBM] or Ln-Si-[ZA/L⊃Tb-AA]. The materials were exposing the vapor of phen or bipy by ship-in-bottle method for about 12 h. The product was obtained after centrifugation and purification obtained the resulting material.

**Preparations of thin film.** The transparent organic-inorganic materials Ln-Si-[ZA/L⊃Eu-DBM]-PEMA/PMMA (Ln-Si-[ZA/L⊃Tb-AA]-PEMA/PMMA) were finally prepared from the radical polymerization of the monomer ethyl methylacryate/methyl methacrylate (EMA/MMA) and the Ln-Si-[ZA/L⊃Eu-DBM] (Ln-Si-[ZA/L⊃Tb-AA]). 1 mL of liquid monomer EMA/MMA and 2 wt % of nano sized modified ZA/L were redispersed in tetrahydrofuran (THF) by stirring for 1 h. Then, 1.1 mg of initiator (AIBN) was added, and the mixture was refluxed at 423 K for 5 h. The luminescent thin films of the assembly of ZA/L were prepared by direct spin-coating through dropping the suspension onto a pre-cleaned glass. The sample was left in the air at room temperature for 24 h to obtain the thin film.

## Results and discussion

The composition and assembly process of photofunctional lanthanide hybrid materials L-Ln-Si-[ZA/L⊃Eu-DBM] and L-Ln-Si-[ZA/L⊃Tb-AA] (acetylacetone = AA, dibenzoylmethane = DBM; Ln = Eu or Tb; L = phen (1,10-phenanthroline), bipy (2,2'-bipyridyl)) are shown in Figure 1. It is difficult to determine the interaction between the functional units in the hybrid materials, and is even hard to determine their exact structures. However, according to the lanthanide coordination chemistry principle, the main framework of these hybrid materials could be predicted. Since rare earth ions have outstanding coordination ability, and we prepare the lanthanide complexes by adding the accurate and appropriate proportion of organic dyes into $Ln^{3+}$ ions. Zeolite A/L have regular and uniform channels (cavities), and organic-lanthanide compounds could be inserted via ion-exchange and ''ship in a bottle method''. The silica coupling agent γ-MPS is chosen in the work because its carbonyl groups can coordinate with $Ln^{3+}$, and the trimethoxysilyl groups could react with OH groups on the surface of ZA/L crystals. Finally, lanthanide ions and phen or bipy are introduced through the coordination interaction among them. The chelation effect between $Eu^{3+}/Tb^{3+}$, γ-MPS and phen (bipy) is easily formed and the molar ratio 1: 2: 2 (1: 2: 2) of $Eu^{3+}/Tb^{3+}$: γ-MPS: phen (bipy) can occupy eight coordination position of $Ln^{3+}$. And the predicted structure of


This journal is © The Royal Society of Chemistry 2012
Photochemical & Photobiological Sciences Accepted Manuscript

the eventual hybrid system was drawn in Figure 1 (d). The double modification of both inside and outside ZA/L host provide the novel path to prepare lanthanide hybrids, which may provide the possibility to further tune the luminescence color. Comparing the simple lanthanide hybrids, this kind of complicated hybrids embodies the possibility to tune the photofunctional performance.

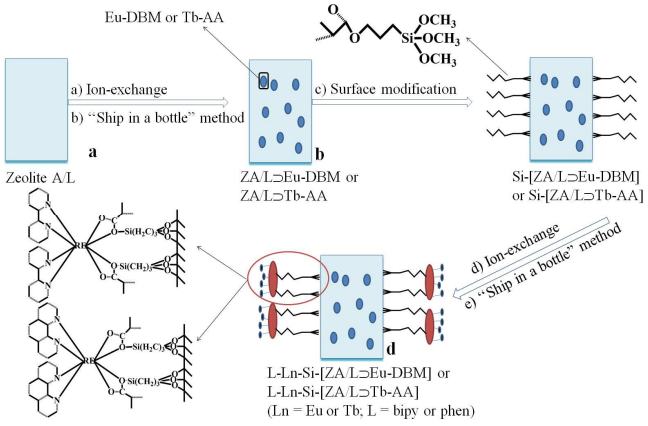


**Figure 1** Schematic representation of microporous materials L-Ln-Si-[ZA/L⊃Eu-DBM] and L-Ln-Si-[ZA/L⊃Tb-AA] (Ln = Eu or Tb; L = bipy or phen).

Figure S1 (a) shows the scanning electron microscopy (SEM) of the cylindrical structure of ZL material and the typical truncated cubes (rhombic dodecahedra). The particle size of zeolite L crystals can be tune in a wide size range of 30 nm to 6000 nm by variation of a convenient standard procedure, and with crystals of different morphology ranging from disc to elongated cylinders.[12] Zeolite A has a three dimensional network with the smallest and the largest free diameters of 0.41 and 1.14 nm, respectively.[6] SEM images of zeolite A are shown in Figure S1 (b) displays an average dimension of 3 um. Figure S2 shows the X-ray diffraction (XRD) patterns of zeolite L (a) and zeolite A (b), and the 2θ-range 5-70 ° for this measurement. In this research, zeolite L and zeolite A show excellent framework structure of crystals. Cations $Na^+$ of zeolite A can be readily exchanged by various ions such as $Ca^{2+}$, $Sr^{2+}$, $Ba^{2+}$, $Zn^{2+}$, $Mn^{2+}$, $Co^{2+}$, $Ni^{2+}$, and the impact of different exchanged ions on the framework stability of zeolite A is diverse.[13] The structure of zeolite L consists of cancrinite cages (Î-cage) linked by double 6-rings (D6R). Only the monovalent cations of zeolite L inside the main channel near the wall of the 8-ring seem to be exchangeable at room temperature in aqueous environment.[14]

The selected FT-IR spectra of γ-MPS functionalized bipy-Eu-Si-[ZL⊃Tb-AA] crystals are shown in Figure S3. It is employed to prove that γ-MPS was successfully immobilized on the surface of $Tb(AA)_n$-ZL. Bands at 1718 and 1645 $cm^{-1}$ were observed in the spectrum, which can be ascribed to the absorption of C=O and C=C of γ-MPS immobilized on the surface of zeolite A/L, thus corroborating that TAA-Si has been successfully grafted onto the external surface of lanthanide loaded zeolite L. Moreover, the peaks at t 1097 ($\upsilon_{as}$, Si-O), 773 ($\upsilon_s$, Si-O) and 475 $cm^{-1}$ (υ, Si-O-Si) were due to the formation of the Si-O-Si framework. The strongest absorption band appearing around 1097 $cm^{-1}$ which was relative to the zeolite L host structure is assigned to anti-symmetric $\upsilon_{as}$ (T–O) stretching vibrations (T = Si or Al). Compared with T-O of zeolite A whose absorption band is around 1000 $cm^{-1}$, the higher wavenumber of zeolite A is due to its lower Al/Si ratio.

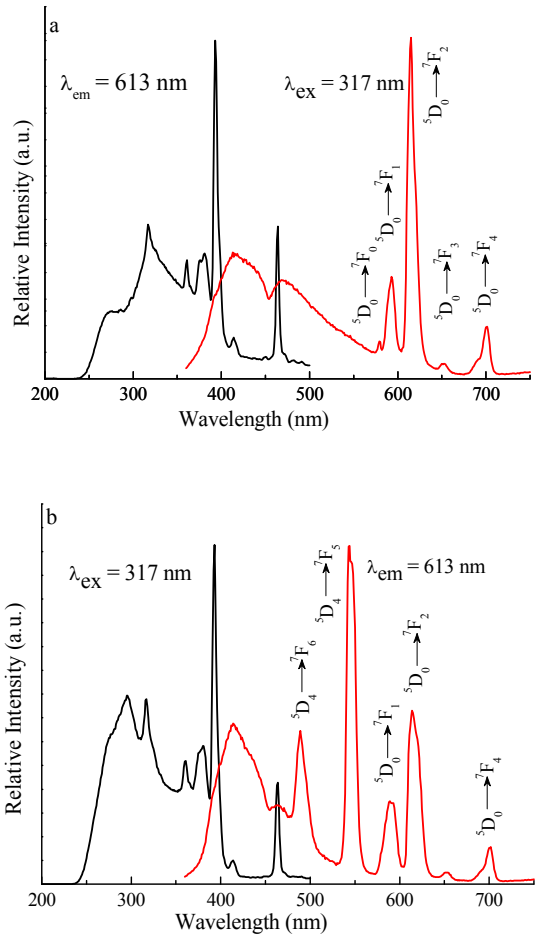


**Figure 2** The excitation and emission spectra of bipy-Eu-Si-[ZA⊃Eu-DBM] (a) and phen-Tb-Si-[ZA⊃Eu-DBM] (b). Excitation spectra observed at 613 nm; emission spectra upon excitation at 317 nm.

Figure 2 shows the excitation and emission spectra of bipy-Eu-Si-[ZA⊃Eu-DBM] (a) and phen-Tb-Si-[ZA⊃Eu-DBM] (b). The excitation spectrum of bipy-Eu-Si-[ZA⊃Eu-DBM] is obtained by monitoring the $^5D_0 \rightarrow {}^7F_2$ transition line at 613 nm, and the emission spectrum of it is obtained by excitation at 317 nm. A broad band ranging from 250 to 400 nm resulting from the π-π* transition of bipy and DBM can be observed in the excitation spectrum, implying that a ligand-to-metal energy transfer takes place in the channels. Furthermore, two strong sharp absorption lines at 393 nm and 464 nm can be observed, which corresponds to $^7F_0 \rightarrow {}^5L_6$ and $^7F_0 \rightarrow {}^5D_2$ of the $Eu^{3+}$ ions, respectively. The emission spectrum of the sample consists of two narrow bands ranging from 370 to 570 nm and three prominent lines at 592, 615 and 701 nm, which can be ascribed to the $^5D_0 \rightarrow {}^7F_1$, $^5D_0 \rightarrow {}^7F_2$, and $^5D_0 \rightarrow {}^7F_4$ transitions, respectively. The hypersensitive forced electronic dipole $^5D_0 \rightarrow {}^7F_2$ transition shows the highest emission intensity. In Figure 2 (b), the excitation spectrum was obtained by monitoring the $^5D_0 \rightarrow {}^7F_2$ transition of $Eu^{3+}$ at 613 nm. A broad emission band about from 250 to 400 nm and five sharp absorption lines at 317, 360, 380, 394 nm and 464 nm can be



Photochemical & Photobiological Sciences Accepted Manuscript

observed. The strongest sharp absorption lines at 394 nm, which correspond to $^7F_0 \rightarrow ^5L_6$ of the $Eu^{3+}$ ions. In the emission spectra ($\lambda_{ex}$ = 317 nm), the characteristic emissions of $Tb^{3+}$ (488 nm, $^5D_4 \rightarrow ^7F_6$; 543 nm, $^5D_4 \rightarrow ^7F_5$) and $Eu^{3+}$ (614 nm, $^5D_0 \rightarrow ^7F_2$; 702 nm, $^5D_0 \rightarrow ^7F_4$) can be obviously observed. The peak at 589 nm may be the overlap of $Eu^{3+}$ (592 nm, $^5D_0 \rightarrow ^7F_1$) and $Tb^{3+}$ (587 nm, $^5D_4 \rightarrow ^7F_4$). A narrow emission band about from 380 to 430 nm peaking at 413 nm can be observed. In addition, comparing Figure 2 (a) with Figure 2 (b), both of them show another similar broad emission band at the range of 350-450 nm, which is originated from the functionalized ZA host. These emission bands at blue and red region (or green for Figure 2b) in the two spectra may be expected to obtain the white light output. Therefore, it can be clearly seen that in the complicated hybrids, multi-component units are easily to select to further tune the luminescent performance of the final material.

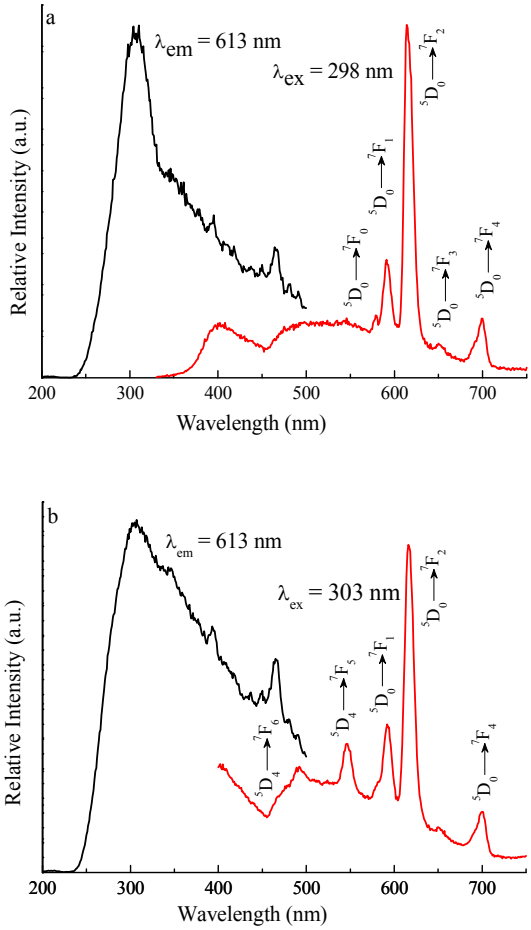


**Figure 3** Excitation and emission spectra of bipy-Eu-Si-[ZL⊃Eu-DBM] (a) and phen-Tb-Si-[ZL⊃Eu-DBM] (b). Excitation spectra were observed at 613 nm, emission spectra upon excitation at 298 nm (a) and 303 nm (b).

Figure 3 shows the luminescence data of bipy-Eu-Si-[ZL⊃Eu-DBM] (a) and phen-Tb-Si-[ZL⊃Eu-DBM] (b). The luminescence data of the bipy-Eu-Si-[ZL⊃Eu-DBM] are shown in Figure 5 (a). The excitation spectra obtained by monitoring the $^5D_0 \rightarrow ^7F_2$ at 613 nm for the hybrid materials show a broad band ranging from 250 to 450 nm peaking at 305 and 310 nm, which can be ascribed to the interaction between organic ligands and $Eu^{3+}$ ions. No obvious absorption lines of $Eu^{3+}$ ions can be observed from the excitation spectra, indicating that an effective energy transfer occurs from DBM to the $Tb^{3+}$ ions. Excitation into this broad band results in three sharp emission lines at 591, 614 and 700 nm, which can be ascribed to the $^5D_0 \rightarrow ^7F_1$, $^5D_0 \rightarrow ^7F_2$, and $^5D_0 \rightarrow ^7F_4$ transitions, respectively. There are two narrow bands ranging from 360 to 455 nm and 455 to 570 nm, which can be ascribed to zeolite A material and bipy, DBM. In Figure 3 (b), there is one weak sharp transition at 466 nm can be observed, which corresponds to $^7F_0 \rightarrow ^5D_2$ of the $Eu^{3+}$ ions. And the hybrid materials show a broad band ranging from 250 to 500 nm peaking at 307 nm. In the emission spectra ($\lambda_{ex}$ = 303 nm), the characteristic emissions of $Tb^{3+}$ (490 nm, $^5D_4 \rightarrow ^7F_6$; 546 nm, $^5D_4 \rightarrow ^7F_5$) and $Eu^{3+}$ (593 nm, $^5D_0 \rightarrow ^7F_1$; 700 nm, $^5D_0 \rightarrow ^7F_4$) can be obviously observed. The peak at 617 nm may be the overlap of $Eu^{3+}$ (613 nm $^5D_0 \rightarrow ^7F_2$) and $Tb^{3+}$ (622 nm, $^5D_4 \rightarrow ^7F_3$). Different from the emission spectra in Figure 2, the wide emission bands for the modified ZL host are not strong in Figure 3, so it can be predicted the blue emission is weak and give rise to the final luminescent color may move to white or cool white region.

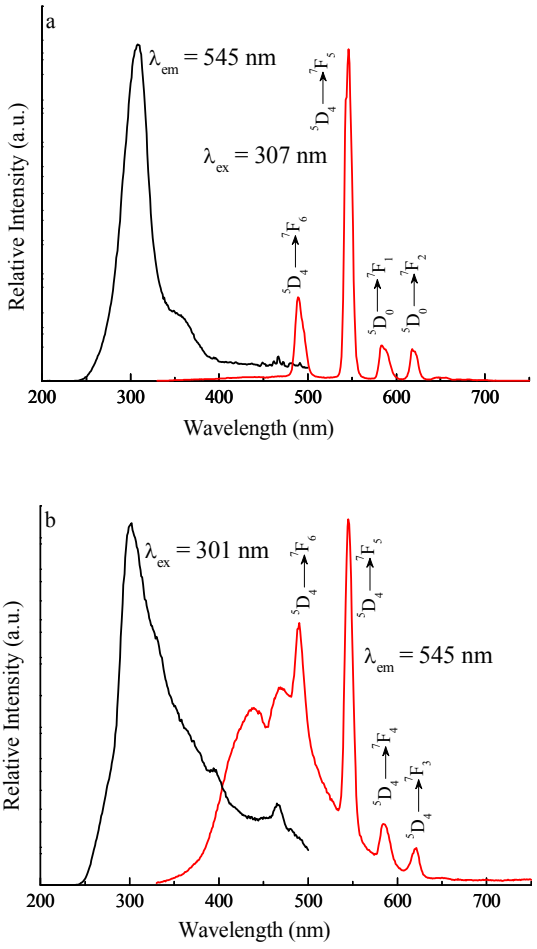


**Figure 4** Excitation and emission spectra of bipy-Eu-Si-[ZL⊃Tb-AA] (a) and phen-Tb-Si-[ZL⊃Tb-AA] (b). Those of 2 were recorded upon excitation at 307 and 301 nm, respectively; emission spectra upon excitation at 545 nm.


This journal is © The Royal Society of Chemistry 2012

Photochemical & Photobiological Sciences Accepted Manuscript

The luminescence data of bipy-Eu-Si-[ZA⊃Tb-AA] and phen-Tb-Si-[ZA⊃Tb-AA] are shown in Figure S4. Figure 4 (a) exhibits the excitation and emission spectra of bipy-Eu-Si-[ZA⊃Tb-AA]. The excitation spectra is measured by monitoring the $^5D_4 \rightarrow {}^7F_5$ transition line of $Tb^{3+}$ at 545 nm and dominated by a broad band about from 250 to 500 nm located in the visible region, one sharp absorption lines at 472 nm can be observed. Excitation of bipy ligand at 342 nm lead to a large broad band from 450 to 750 nm in the visible light region and characteristic weak band at 545 nm is attributed to f-f transition of $Tb^{3+}$ ($^5D_4 \rightarrow {}^7F_5$). Figure 4(b) shows the luminescent spectra of phen-Tb-Si-[ZA⊃Tb-AA]. A complicated excitation spectrum monitored with the $^5D_4 \rightarrow {}^7F_5$ transition at 545 nm is composed of a broad absorption band and several excitation lines, which correspond to characteristic absorption of the $\pi$-$\pi^*$ electron transition and ineffective energy transfer occurring form dyes to $Tb^{3+}$. The emission spectrum is obtained u 327 nm, which exhibits a broad band about from 400 to 700 nm and four sharp emission lines at 490, 545, 583 and 623 nm attributed to $^5D_4 \rightarrow {}^7F_J$ (J = 6-3) respectively.

Figure 4 (a) displays the selected excitation and emission spectra of bipy-Eu-Si-[ZL⊃Tb-AA] hybrids. In the excitation spectra, a broad band centered at 307 m with shoulder at 357 nm was observed, which is characteristic absorption of AA due to the $\pi$-$\pi^*$ electron transition. It indicates that an energy transfer occurs from AA to the central $Tb^{3+}$. The emission spectra excited at 307 nm shows characteristic sharp bands at 489, 546 and 583 nm attributed to the f–f transition of $Tb^{3+}$ ($^5D_4 \rightarrow {}^7F_J$, J = 6, 5, 4), sharp band at 618 nm attributed to and the overlap of $Eu^{3+}$ (613 nm $^5D_0 \rightarrow {}^7F_2$) and $Tb^{3+}$ (622 nm $^5D_4 \rightarrow {}^7F_3$). The half-width of the strongest bands is less than 15 nm, indicating that the bipy-Eu-Si-[ZL⊃Tb-AA] materials exhibit high fluorescence intensity and color purity. While for the luminescent spectra of phen-Tb-Si-[ZL⊃Tb-AA] hybrids in Figure 4(b) with the same excitation wavelength, it shows distinctively different band to Figure 4(a). For its excitation spectra, only a strong broad emission band with shoulder at 394 and 466 nm was observed. The emission spectrum is obtained by detecting the strongest band of 301 nm. A strong broad emission band is checked in the visible region centered at 439 and 467 nm for the modified host, and strong characteristic emission of $Tb^{3+}$ with sharp bands at 490, 545, 584 and 621 nm attributed to $^5D_4 \rightarrow {}^7F_J$ (J = 6-3) appears.

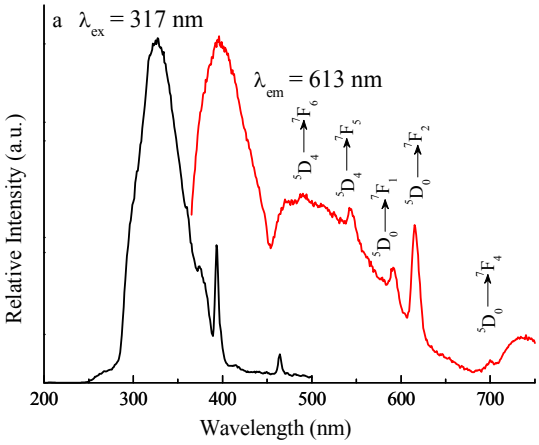


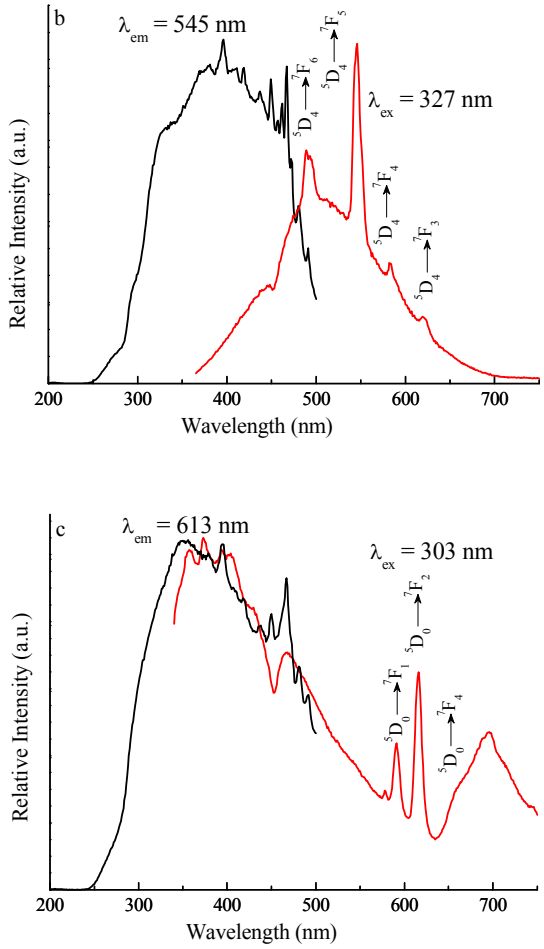


**Figure 5** The digital photos of phen-Tb-Si-[ZA⊃Eu-DBM]-PMMA (A, a), phen-Tb-Si-[ZA⊃Tb-AA]-PMMA (B, b) and phen-Tb-Si-[ZL⊃Eu-DBM]-PEMA (C, c) under visible region and UV irradiation ($\lambda_{ex}$ = 365nm).

Package polymer can effectively protect the guest species inside and outside of the nano-channels of ZA/L. The luminescent spectra of thin films are shown in Figure 5. Figure 5(a) for luminescent spectra of phen-Tb-Si-[ZA⊃Eu-DBM]-PMMA is measured by monitoring the luminescence intensity of the $^5D_0$ - $^7F_2$ transition at 613 nm of $Eu^{3+}$. The excitation spectrum of phen-Tb-Si-[ZA⊃Eu-DBM]-PMMA is composed of a broad band from 250 to 400 nm and two absorption lines at 393 nm and 464 nm. The strong sharp absorption lines at 393 nm correspond to $^7F_0 \rightarrow {}^5L_6$ of the $Eu^{3+}$ ions. Compared with phen-Tb-Si-[ZA⊃Eu-DBM] (Figure 4(b)), the characteristic excitation lines of lanthanide ions are relatively less and the emission band of phen and DBM ligands within the channels of the ZA crystals that are wrapped in polymers are significantly enhanced. phen-Tb-Si-[ZA⊃Eu-DBM]-PMMA shows very similar emission spectral features to the phen-Tb-Si-[ZA⊃Eu-DBM], no obvious shift in the wavelength of the emission lines ($\lambda_{ex}$ = 317 nm) can be observed as revealed by comparing Figure 5(a) with Figure 4(b). The luminescent spectra of phen-Tb-Si-[ZA⊃Tb-AA]-PMMA is shown in Figure 5(b). The excitation spectrum is obtained when monitored with the $^5D_4 \rightarrow {}^7F_5$ transition of $Tb^{3+}$ at 545 nm, which exhibits a broad band from 250 to 500 nm and several sharp

Photochemical & Photobiological Sciences Accepted Manuscript

absorption lines. The emission spectrum is obtained when excited at 327 nm. No significant changes are observed in the emission spectrum between phen-Tb-Si-[ZA⊃Tb-AA]-PMMA] and phen-Tb-Si-[ZA⊃Tb-AA] as shown in Figure 5(b) and 6(b). Figure 5(c) represents the excitation and emission spectra of phen-Tb-Si-[ZL⊃Eu-DBM]-PEMA. When compared with the excitation spectra of phen-Tb-Si-[ZL⊃Eu-DBM], phen-Tb-Si-[ZL⊃Eu-DBM]-PEMA has a stronger sharp transition at 467 nm can be observed, which corresponds to $^7F_0 \rightarrow {}^5D_2$ of the $Eu^{3+}$ ions. In the emission spectra ($\lambda_{ex}$ = 303 nm), the characteristic emissions of $Eu^{3+}$ (593 nm, $^5D_0 \rightarrow {}^7F_1$; 700 nm, $^5D_0 \rightarrow {}^7F_4$) are remain, however the emissions lines of $Tb^{3+}$ is disappear. And the thin film materials have two broad bands ranging from 340 to 450 nm and 635 to 750 nm, ascribed to the effect of organic ligand.

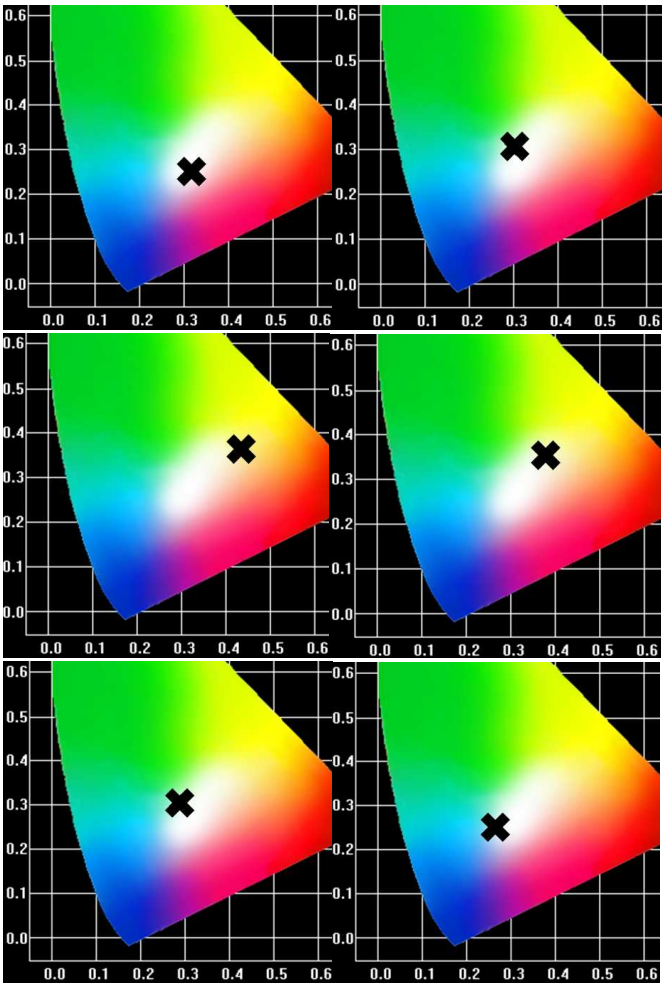

**Figure 6** The selected CIE diagrams for hybrid materials: from left-right, top-bottom a-f: a for bipy-Eu-Si-[ZA⊃Eu-DBM] ($\lambda_{ex}$ = 317 nm), b for phen-Tb-Si-[ZA⊃Eu-DBM] ($\lambda_{ex}$ = 317 nm), c for bipy-Eu-Si-[ZL⊃Eu-DBM] ($\lambda_{ex}$ = 298 nm), d for phen-Tb-Si-[ZL⊃Eu-DBM] ($\lambda_{ex}$ = 303 nm), e for phen-Tb-Si-[ZA⊃Eu-DBM]-PMMA ($\lambda_{ex}$ = 365 nm), and f for phen-Tb-Si-[ZL⊃Eu-DBM]-PEMA ($\lambda_{ex}$ = 365 nm).

The corresponding CIE coordinates diagrams of the hybrid materials are shown in the following Figure 6. Figure 6 (a) for bipy-Eu-Si-[ZA⊃Eu-DBM] ($\lambda_{ex}$ = 317 nm) is situated at close white region, whose CIE coordinate is (x = 0.3221, y = 0.2529). Figure 6 (b) for phen-Tb-Si-[ZA⊃Eu-DBM] ($\lambda_{ex}$ = 317 nm) is located in white region, whose CIE coordinate is (x = 0.3035, y = 0.2976). So the introduction of $Tb^{3+}$ emission is benefit for the white light output, which takes agreement with the results of Figure 2. Figure 6 (c) and 6 (d) show that the corresponding CIE coordinates of the hybrid materials (bipy-Eu-Si-[ZL⊃Eu-DBM] and phen-Tb-Si-[ZL⊃Eu-DBM]) are (x = 0.4309, y = 0.3627) and (x = 0.3771, y = 0.3609), respectively. The relatively weak emission in blue region for functionalized ZL make the luminescence color to shift to cool white region, especially white luminescence for phen-Tb-Si-[ZL⊃Eu-DBM]), which is useful for lighting. Figure 6 (e) and 6 (f) show the selected CIE diagrams for the two hybrid polymer films phen-Tb-Si-[ZA⊃Eu-DBM]-PMMA (x = 0.2776, y = 0.3093) and phen-Tb-Si-[ZL⊃Eu-DBM]-PEMA (x = (x = 0.2623, y = 0.2548), respectively, both of which show the strong emission of modified ZA/L host and the weak emission of lanthanide species. The luminescence color is in near white region (light blue color) like Figure 6 (b), among phen-Tb-Si-[ZA⊃Eu-DBM]-PMMA can emit white luminescence. The corresponding CIE coordinates of the other hybrid materials are shown in Figure S5 of ESI, which cannot obtain white light. Therefore, by adjusting the different component of the hybrid system, it can realize the tuning and integrating of luminescence color.

**Table 1** The luminescence data of the hybrid materials.

| Materials | $\lambda_{ex}$ ($\lambda_{em}$) | $\tau$ (μs) | $\eta$ (%) |
|---|---|---|---|
| bipy-Eu-Si-[ZA⊃Eu-DBM] | 613 | 557 | 15 |
| phen-Tb-Si-[ZA⊃Eu-DBM] | 613 | 465 | 32 |
| bipy-Eu-Si-[ZL⊃Eu-DBM] | 613 | 527 | 4.4 |
| phen-Tb-Si-[ZL⊃Eu-DBM] | 613 | 374 | 26 |
| bipy-Eu-Si-[ZA⊃Tb-AA] | 545 | 274 | 2.1 |
| phen-Tb-Si-[ZA⊃Tb-AA] | 545 | 306 | 5.8 |
| bipy-Eu-Si-[ZL⊃Tb-AA] | 545 | 218 | 25 |
| phen-Tb-Si-[ZL⊃Tb-AA] | 545 | 534 | 31 |

$\tau$, lifetime for $^5D_4 \rightarrow {}^7F_5$ transition of $Tb^{3+}$ and $^5D_0 \rightarrow {}^7F_2$ transition of $Eu^{3+}$; $\eta$, the emission quantum efficiency.

To further investigate the luminescence property of these multi-component hybrid materials, their emission quantum efficiency and the luminescent lifetimes for dominant emissive $Tb^{3+}$ ($^5D_4 \rightarrow {}^7F_5$) or $Eu^{3+}$ ($^5D_0 \rightarrow {}^7F_2$) are measured, whose data are given in Table 1. We can see from the lifetime data that the same $Tb^{3+}$ ($^5D_4 \rightarrow {}^7F_5$) or $Eu^{3+}$ ($^5D_0 \rightarrow {}^7F_2$) emission of inside-outside modified hybrid materials are longer than those of the different lanthanide ions modified ones, suggesting the cooperating luminescence of the same luminescent $Ln^{3+}$. The luminescent quantum yields data show no clear rule for the complicated composition of these hybrid materials. Because there are several luminescent units in the whole hybrid systems and the absolute luminescent quantum yields are contributed by the total integration. This makes the quantum yields data show no apparent rule. It needs to be referred that the hybrids with Tb-phen unit possess the higher quantum yields than those with Eu-bipy one, which may be due to the energy match between phen and $Tb^{3+}$ is more effective than bipy and $Eu^{3+}$. This perhaps due to the energy match between phen and $Tb^{3+}$ is more effective than bipy and $Eu^{3+}$.

Photographs of the hybrid material with a content of 2 wt% zeolite A/L are shown in Figure 7, which reveals that the obtained polymer hybrid films are transparent and show characteristic

Photochemical & Photobiological Sciences Accepted Manuscript


This journal is © The Royal Society of Chemistry 2012

emission under UV illumination ($\lambda_{ex}$ = 365 nm). SEM images of phen-Tb-Si-[ZL⊃Eu-DBM-ZL]-PEMA (a), phen-Tb-Si-[ZA⊃Tb-AA-ZL]-PMMA (b) and phen-Tb-Si-[ZA⊃Eu-DBM-ZL]-PMMA (c) are shown in Figure S6. There are several white spots are evenly distributed on the smooth background of the PEMA/PMMA polymer originated from zeolite A/L. The surface images of the transparent materials and cross-sectional of phen-Tb-Si-[ZA⊃Tb-AA-ZL]-PMMA (d) explain a homogeneous dispersion of zeolite crystals throughout the polymer matrix.

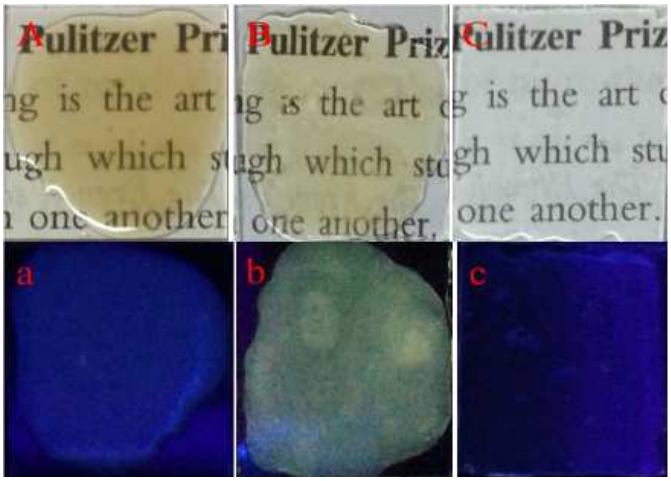


**Figure 7** The digital photos of phen-Tb-Si-[ZL⊃Eu-DBM-ZL]-PEMA (A, a), phen-Tb-Si-[ZA⊃Tb-AA-ZL]-PMMA (B, b) and phen-Tb-Si-[ZA⊃Eu-DBM-ZL]-PMMA (A, a) under visible region and UV irradiation ($\lambda_{ex}$ = 365nm).

Figure S7 (a) presents the selected ultraviolet-visible diffuse reflective absorption spectra (UV-vis DRS) of hybrids with $Eu^{3+}$ loaded zeolites A, bipy-Eu-Si-[ZA⊃Eu-DBM] (A) and phen-Tb-Si-[ZA⊃Eu-DBM] (B). It is found that both of them show obvious broad absorption band from 250 to 400 nm, which partially overlaps with the excitation spectrum. Figure S6b) presents the UV–vis DRS of hybrids bipy-Tb-Si-[ZL⊃Eu-DBM] (C) and phen-Eu-Si-[ZL⊃Eu-DBM] (D). Both of them show a large absorption band from 250 to 350 nm and a large emission band from 350 to 650 nm, which overlaps with the luminescent spectrum of $Eu^{3+}$ complexes loaded zeolites L. Absorption band in this spectra indicates that major π-π* electronic transitions of the organic dyes. UV-vis DRS of bipy-Tb-Si-[ZA⊃Tb-AA] (E) and phen-Eu-Si-[ZA⊃Tb-AA] (F) are shown in Figure S6(c). Obvious absorption band at ultraviolet region and emission band at visible region can be proved in their emission and excitation spectra. bipy-Eu-Si-[ZL⊃Tb-AA] (G) shows a large absorption band from 250 to 400 nm and emission band at visible region, that is overlaps with its luminescent spectrum. The emission band of phen-Tb-Si-[ZL⊃Tb-AA] from 400 to 550 nm represents the effect of organic ligand, and the absorption band is overlaps with its excitation spectra.

## Conclusions

In summary, novel photofunctional hybrid materials are prepared by inside-outside double modification of zeolite A/L with lanthanide complexes. Moreover, thin films are further prepared by the fabrication of them into polymer host. Though properly controlling different building units in the hybrid systems, the luminescence color can be tuned. Some of which can be integrated to obtain white light output. These results provide useful path to prepare multi-component lanthanide hybrid materials and further adjust their luminescence, which may be expected to have potential applications in the future.

## Acknowledgements

This work is supported by the National Natural Science Foundation of China (91122003, 20971100), the Program for New Century Excellent talents in University (NCET-08-0398) and the Developing Science Funds of Tongji University.

## Notes and references

*Department of Chemistry, Tongji University, Shanghai 200092, China.*
*Fax: +86-21-65982287; Tel: +86-21-65984663;*
*E-mail: byan@tongji.edu.cn*

Electronic Supplementary Information (ESI) available: [details of any supplementary information available should be included here]. See DOI: 10.1039/b000000x/

1. (*a*) Z. Li, G. Luppi, A. Geiger, H. P. Josel and L. De Cola, *Small*, 2011, **7**, 3193; (*b*) G. De Cremer, B. F. Sels, J. i. Hotta, M. B. Roeffaers, E. Bartholomeeusen, E. Coutiño‐Gonzalez, V. Valtchev, D. E. De Vos, T. Vosch and J. Hofkens, *Adv. Mater.*, 2010, **22**, 957; (c) S. Comby and J.-C. G. Bünzli, *Handb. Phys. Chem Rare Earths*, 2007, **37**, 217; (*d*). P. Escribano, B. Julián-López, J. Planelles-Aragó, E. Cordoncillo, B. Viana and C. Sanchez, *J. Mater. Chem*., 2008, **18**, 23; (*e*) L. D. Carlos, R. A. Ferreira, V. d. Z. Bermudez and S. J. Ribeiro, *Adv. Mater*., 2009, **21**, 509.
2. (*a*) K. Binnemans, *Chem. Rev.*, 2009, **109**, 4283; (*b*) B. Yan, *RSC Adv.*, 2012, **2**, 9304; (*c*) J. Feng, H. J. Zhang, *Chem. Soc. Rev.*, 2013, **42**, 387; (*d*) L. D. Carlos, R. A. Ferreira, V. D. Bermudez, B. Julián-López and P. Escribano, *Chem. Soc. Rev.*, 2011, **40**, 536.
3. (*a*) L. Sun, W. Mai, S. Dang, Y. Qiu, W. Deng, L. Shi, W. Yan and H. Zhang, *J. Mater. Chem.*, 2012, **22**, 5121; (*b*) Y. Li, B. Yan and X. Qiao, *Microp. Mesop. Mater.*, 2013, **163**, 60; (*c*) J. Feng, S. Y. Song, W. Q. Fan, L. N. Sun, X. M. Guo, C. Y. Peng, J. B. Yu, Y. N. Yu and H. J. Zhang, *Microp. Mesop. Mater.*, 2009, **117**, 278; (*d*) B. Yan and Y.-J. Gu, *Inorg. Chem. Commun.*, 2013, **34**, 75.
4. (*a*) Y. Li, B. Yan and H. Yang, *J. Phys. Chem. C*, 2008, **112**, 3959; (*b*) Y. J. Li, B. Yan and L. Wang, *Dalton Trans.*, 2011, **40**, 6722; (*c*) Y. J. Li, B. Yan, *Dalton Trans.*, 2010, **39**, 2554; (*d*) B. Yan, Y. Y. Li and X. F. Qiao, *Microp. Mesop. Mater.*, 2012, **158**, 129.
5. H. V. Bekkum, J. Jansen and E. *Flanigen*, Introduction to Zeolite Science and Practice Elsevier: Amsterdam, 1991.
6. (*a*) H. Li, Y. Ding, P. Cao, H. Liu and Y. Zheng, *J. Mater. Chem.*, 2012, **22**, 4056; (*b*) V. Vohra, A. Devaux, L. Q. Dieu, G. Scavia, M. Catellani, G. Calzaferri and C. Botta, *Adv. Mater.*, 2009, **21**, 1146; (*c*) M. Busby, C. Blum, M. Tibben, S. Fibikar, G. Calzaferri, V. Subramaniam and L. De Cola, *J. Am. Chem. Soc.*, 2008, **130**, 10970.
7. (*a*) A. Zabala Ruiz, H. Li and G. Calzaferri, *Angew. Chem., Int. Ed*., 2006, **118**, 5408; (*b*) A. Mech, A. Monguzzi, F. Meinardi, J. Mezyk, G. Macchi and R. Tubino, *J. Am. Chem. Soc.*, 2010, **132**, 4574.
8. (a) P. Li, D. Wang, D. Liang, L. Zhang, S. Zhang and Y. Wang, *Mater. Res. Bull.*, 2014, **55**, 216; (*b*) H. Li, H. Zhang, L. Wang, D. Mu, S. Qi, X. Hu, L. Zhang and J. Yuan, *J. Mater. Chem*., 2012, **22**, 9338; (*c*) Y. Wang, H. Li, W. Zhang and B. Liu, *Mater. Lett.*, 2008, **62,** 3167.
8. Y. Wang, H. Li, L. Gu, Q. Gan, Y. Li and G. Calzaferri, *Microporous Mesoporous Mater.*, 2009, **121**, 1.
9 (*a*) J. N. Hao and B. Yan, *Dalton Trans.*, 2014, **43**, 2810; (*b*) J. N. Hao and B. Yan, *New J. Chem*., 2014, **38**, 3540; (*c*) L. Chen and B. Yan, Dalton Trans., 2014, **43**, 14123.
10. S. Suárez, A. Devaux, J. Bañuelos, O. Bossart, A. Kunzmann and G. Calzaferri, *Adv. Funct. Mater.*, 2007, **17**, 2298.
11. (*a*) P. Lainé, R. Seifert, R. Giovanoli and G. Calzaferri, *New J. Chem.*, 1997, **21**, 453; (b) A. Z. Ruiz, D. Brühwiler, T. Ban and G. Calzaferri, *Monatsh. Chem.,* 2005, **136**, 77.
12. S. S. Hassani, F. Salehirad, H. Aghabozorg and Z. Sobat, *Cryst. Res. Technol.*, 2010, **45**, 183.

Photochemical & Photobiological Sciences Accepted Manuscript

13. (*a*) I. Gal, O. Janković, S. Malčić, P. Radovanov and M. Todorović, *Trans. Faraday Soc.*, 1971, **67**, 999; (b) D. Breck, W. Eversole, R. Milton, T. Reed and T. Thomas, *J. Am. Chem. Soc.*, 1956, **78**, 5963.
14. (a) B. Hennessy, S. Megelski, C. Marcolli, V. Shklover, C. Bärlocher and G. Calzaferri, *J. Phys. Chem. B.*, 1999, **103**, 3340; (*b*) A.Burton and R. F. Lobo, *Microp. Mesop. Mater.*, 1999, **33**, 97.

Photochemical & Photobiological Sciences Accepted Manuscript


This journal is © The Royal Society of Chemistry 2012

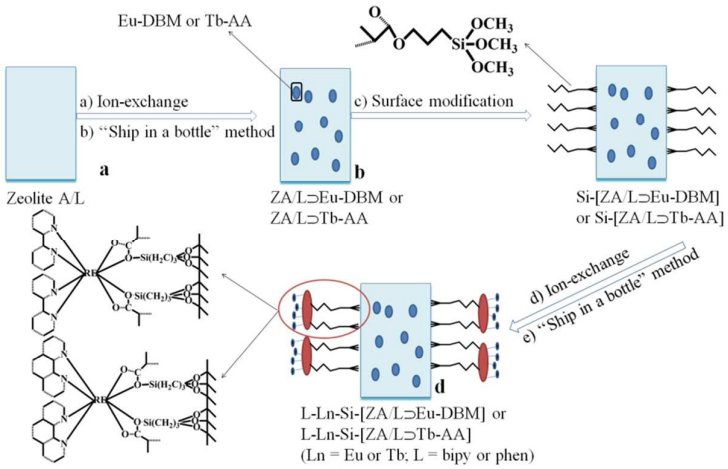


Some multi-component hybrids based zeolite L/A are prepared by an inner-outside double modifications path for ZA/L with lanthanide complexes. Some of which display white or near-white light emission. Furtherly, selected above hybrids are fabricated into PEMA/PMMA (poly ethyl methylacryate/poly methyl methacrylate) host to prepare luminescent polymer films. These results provide abundant data to be expected to have potential application in various practical fields.

Photochemical & Photobiological Sciences Accepted Manuscript